JACS
JOURNAL OF THE AMERICAN CHEMICAL SOCIETY
pubs.acs.org/JACS
Article

QM/MM Modeling of Vibrational Polariton Induced Energy Transfer and Chemical Dynamics

Tao E. Li* and Sharon Hammes-Schiffer*

Cite This: https://doi.org/10.1021/jacs.2c10170
Read Online
ACCESS | Metrics & More | Article Recommendations | Supporting Information

ABSTRACT: Vibrational strong coupling (VSC) provides a novel means to modify chemical reactions and energy transfer pathways. To efficiently model chemical dynamics under VSC in the collective regime, herein a hybrid quantum mechanical/molecular mechanical (QM/MM) cavity molecular dynamics (CavMD) scheme is developed and applied to an experimentally studied chemical system. This approach can achieve linear scaling with respect to the number of molecules for a dilute solution under VSC by assuming that each QM solute molecule is surrounded by an independent MM solvent bath. Application of this approach to a dilute solution of $Fe(CO)_5$ in *n*-dodecane under VSC demonstrates polariton dephasing to the dark modes and polariton-enhanced molecular nonlinear absorption. These simulations predict that strongly exciting the lower polariton may provide an energy transfer pathway that selectively excites the equatorial CO vibrations rather than the axial CO vibrations. Moreover, these simulations also directly probe the cavity effect on the dynamics of the $Fe(CO)_5$ Berry pseudorotation reaction for comparison to recent two-dimensional infrared spectroscopy experiments. This theoretical approach is applicable to a wide range of other polaritonic systems and provides a tool for exploring the use of VSC for selective infrared photochemistry.

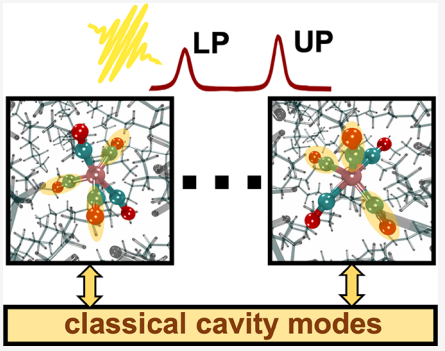

INTRODUCTION

An intriguing finding over the past decade has been the discovery and characterization of molecular vibrational polaritons.[1,2] These hybrid light−matter states were initially observed when a large ensemble of molecules is confined in a Fabry−Pérot cavity, an optical device composed of a pair of parallel mirrors supporting infrared (IR) standing electromagnetic waves. When one standing wave, also known as a cavity mode, is near resonant with one vibrational mode of the molecules, peak splitting, or Rabi splitting, may be observed in the IR spectrum. The Rabi splitting is a hallmark of the formation of vibrational polaritons. Under this vibrational strong coupling (VSC) domain, molecular properties may be significantly modified, including ground-state chemical reaction rates[3,4] and supramolecular assembly[5] under thermal conditions, as well as intermolecular vibrational energy transfer rates under external pumping of the upper polariton (UP).[6] Note that challenges associated with reproducing some of the experiments under thermal conditions have been reported.[7,8]

In parallel with the exciting experimental progress of vibrational polaritons, the theoretical modeling of VSC has moved forward[9−11] but faces significant challenges. A major challenge on the theory side is the collective nature of polaritons versus the locality of chemical modifications.[12] Although vibrational polaritons are formed among a macroscopic number (i.e., $N \sim 10^{10}$) of molecules, many calculations of polariton effects have been performed on single-molecule VSC and therefore are not directly applicable to the collective regime. In the collective regime, each individual molecule makes a negligible contribution to the polariton and predominantly contributes to the dark modes, which are inactive with respect to electromagnetic fields. Understanding how the collective polaritonic state can induce a significant modification of local molecular properties, especially the chemical reaction rates, requires methods beyond conventional chemical modeling of molecules. Many different theoretical efforts, including the study of classical or quantum mechanical model systems,[13−18] quantum-electrodynamical electronic structure theory,[19−24] exaction factorization,[25] and the multiconfigurational time-dependent Hartree method (MCTDH),[26] have been directed toward modeling vibrational polaritons and their chemical effects.

Another appealing approach for modeling VSC is classical cavity molecular dynamics (CavMD) simulations,[27] in which a few cavity modes coupled to a large ensemble of realistic molecules described by empirical force fields are propagated classically on an electronic ground-state surface. Beyond classical simulations, nuclear and photonic quantum effects

Received: September 23, 2022

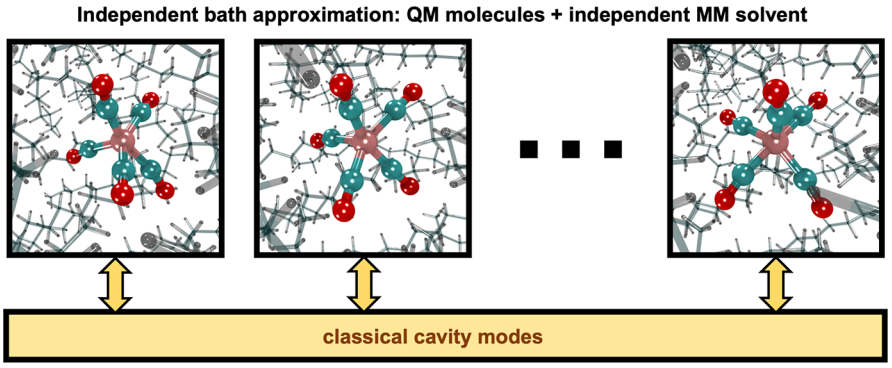

Figure 1. Illustration of the independent bath approximation for simulating collective VSC. The classical cavity modes interact with N_b independent molecular systems, each of which contains a single QM molecule immersed in an MM solvent bath. In this work, we simulate 16 $Fe(CO)_5$ solute molecules forming VSC with a cavity mode, where each solute molecule is surrounded by 50 *n*-dodecane MM molecules. At each time step, the cavity modes interact with the total dipole moment summed over all the independent molecular subsystems, and the dynamics of the molecular subsystems are propagated in parallel. See the Supporting Information for simulation details.

can be included in CavMD by path integral techniques.[28] CavMD has exhibited significant advantages for describing VSC, including the scalability of modeling a large number of molecules as well as agreement with some key experiments and analytic theory.[29] One major limitation of this approach, however, is the inability to model chemical reactions under VSC. The main source of difficulty is that CavMD requires not only nuclear forces but also molecular dipole moments and dipole derivatives during the time propagation. Although dipole derivatives may be approximated as being constant near equilibrium molecular geometries,[27,30] during chemical reactions this approximation may break down, as bond breaking and formation usually lead to very large changes in the dipole derivatives. In contrast, when electronic structure theory is used to calculate dipole derivatives on the fly as second-order energy gradients,[31] the computational cost may become overwhelmingly expensive, especially when the molecular system size is large. Hence, for realistic modeling of ground-state chemical reactions under collective VSC, further approximations are required to reduce the computational cost.

Herein, we develop an efficient CavMD approach with linear scaling for dilute solutions under VSC when only the solute molecules can undergo chemical reactions. In this approach, the molecules are described at the hybrid quantum mechanical/molecular mechanical (QM/MM) level,[32,33] in which the solvent molecules are described by MM with empirical force fields, and the solute molecules are described by QM with electronic structure theory. Because the solute concentration is low, we further assume no direct solute−solute interactions and invoke the independent bath approximation. As illustrated in Figure 1, under the independent bath approximation, the cavity modes interact with N_b independent molecular systems, each of which contains a single QM solute molecule surrounded by a MM solvent bath. Because the QM solute molecules are assumed to have no direct interactions with each other, their gradients can be evaluated independently and also in parallel, leading to linear scaling with respect to the number of QM molecules. The idea of the independent bath approximation was introduced in VSC by del Pino et al.[34] in a fully quantum mechanical model study. The multiscale molecular dynamics scheme for exciton−polaritons developed by Luk et al.[30,35,36] also assumed the independent bath approximation.

We apply this QM/MM CavMD approach to a dilute $Fe(CO)_5$ solution in *n*-dodecane under VSC. The choice of this molecular system was inspired by a recent two-dimensional infrared (2D-IR) spectroscopy experiment performed by Chen et al.[37] Among many VSC chemical reaction experiments,[3,4,38] this 2D-IR experiment reported the simplest reaction under VSC, namely the Berry pseudorotation reaction.[39,40] In addition, this experiment probed the VSC effects on the vibrational energy exchange dynamics between equatorial and axial vibrational modes. After photoexcitation of the polaritons and initial relaxation, the intramolecular vibrational energy redistribution (IVR) between the equatorial and axial vibrational modes was found to be enhanced, whereas pseudorotation was suppressed, compared to the same molecular system outside the cavity.[37] These intriguing VSC effects suggest that polariton relaxation may produce a different initial distribution of the dark modes than the distribution of vibrational modes outside the cavity.[37] To better understand this experiment, which focused on the dynamics after the initial relaxation of the UP (i.e., after ∼2 ps), we use the QM/MM CavMD approach to study the short-time polariton relaxation dynamics (within ∼2 ps) and investigate the resulting dark-mode distribution. Our simulations show that the QM/MM CavMD approach not only reveals polariton dephasing to the dark modes as well as polariton-enhanced molecular nonlinear absorption[41] but also predicts intriguing polariton induced vibrational energy transfer from the axial to the equatorial CO vibrations in $Fe(CO)_5$. Moreover, this approach can also directly simulate the cavity effect on the $Fe(CO)_5$ Berry pseudorotation reaction[39,40] dynamics. Note that the previously developed force field CavMD approach cannot describe such reaction dynamics or the breaking and forming of chemical bonds, a distinct advantage of the QM/MM CavMD approach. To the best of our knowledge, this study represents the first on-the-fly first-principles simulation of VSC chemical dynamics in the collective regime.

THEORY AND METHODS

CavMD Scheme. Under VSC, because the electronic motion is much faster than the dynamics of the nuclei and IR cavity modes, the coupled nuclear−photonic dynamics can be propagated on an electronic ground-state surface. With this cavity Born−Oppenheimer approximation,[42] the light−matter Hamiltonian for CavMD is defined as[27]

$$\hat{H}^{\mathrm{G}}_{\mathrm{QED}} = \hat{H}^{\mathrm{G}}_{\mathrm{M}} + \hat{H}^{\mathrm{G}}_{\mathrm{F}} \tag{1a}$$

https://doi.org/10.1021/jacs.2c10170
J. Am. Chem. Soc. XXXX, XXX, XXX−XXX

where $\hat{H}_{\mathrm{M}}^{\mathrm{G}}$ is the conventional ground-state molecular (kinetic + potential) Hamiltonian outside a cavity, and $\hat{H}_{\mathrm{F}}^{\mathrm{G}}$ denotes the field-related Hamiltonian under the long wave approximation:

$$\hat{H}_{\mathrm{F}}^{\mathrm{G}} = \sum_{k,\lambda} \frac{\hat{\tilde{p}}_{k,\lambda}^{\,2}}{2m_{k,\lambda}} + \frac{1}{2} m_{k,\lambda} \omega_{k,\lambda}^{\,2} \left(\hat{\tilde{q}}_{k,\lambda} + \frac{\epsilon_{k,\lambda}}{m_{k,\lambda}\omega_{k,\lambda}^{\,2}} \hat{d}_{g,\lambda} \right)^2 \tag{1b}$$

Here, $\hat{\tilde{p}}_{k,\lambda}$, $\hat{\tilde{q}}_{k,\hat{\jmath}}$, $\omega_{k,\lambda}$, and $m_{k,\lambda}$ denote the momentum operator, position operator, frequency, and auxiliary mass for the cavity photon mode defined by a wave vector $\mathbf{k}$ and polarization direction $\boldsymbol{\xi}_\lambda$ with $\mathbf{k}\cdot\boldsymbol{\xi}_\lambda = 0$. By construction, the cavity is placed along the z-direction, so $\boldsymbol{\xi}_\lambda$ can be $\mathbf{e}_x$ or $\mathbf{e}_y$, the unit vector along the x- or y-direction. $\hat{d}_{g,\lambda}$ denotes the electronic ground-state dipole operator for the entire molecular system projected along the direction of $\boldsymbol{\xi}_\lambda$. The quantity $\epsilon_{k,\lambda} \equiv \sqrt{m_{k,\lambda}\omega_{k,\lambda}^{\,2}/\Omega\epsilon_0}$ characterizes the coupling strength between each cavity photon and individual molecule, where Ω denotes the cavity mode volume and ϵ_0 denotes the vacuum permittivity.

In classical CavMD, all quantum operators in eqs 1a and 1b are mapped to classical variables. Moreover, in order to use a relatively small molecular system to simulate VSC, which may involve a macroscopic number of molecules, we also assume that the entire molecular system can be represented by N_{cell} identical simulation cells;[27] i.e., the total molecular dipole moment is represented by $d_{g,\lambda} = N_{\mathrm{cell}} d_{g,\lambda}^{\mathrm{sub}}$, where $d_{g,\lambda}^{\mathrm{sub}}$ denotes the molecular dipole moment in a simulation cell. By also denoting $\tilde{\tilde{q}}_{k,\lambda} = \tilde{q}_{k,\lambda}/\sqrt{N_{\mathrm{cell}}}$ and an effective light−matter coupling strength

$$\tilde{\epsilon}_{k,\lambda} \equiv \sqrt{N_{\mathrm{cell}}}\,\epsilon_{k,\lambda} = \sqrt{\frac{N_{\mathrm{cell}} m_{k,\lambda}\omega_{k,\lambda}^{\,2}}{\Omega\epsilon_0}} \tag{2}$$

we obtain classical equations of motion for the coupled photon−nuclear system:

$$M_\alpha \ddot{\mathbf{R}}_\alpha = \mathbf{F}_\alpha^{(0)} + \mathbf{F}_\alpha^{\mathrm{cav}} \tag{3a}$$

$$m_{k,\lambda}\ddot{\tilde{\tilde{q}}}_{k,\lambda} = -m_{k,\lambda}\omega_{k,\lambda}^{2}\tilde{\tilde{q}}_{k,\lambda} - \tilde{\epsilon}_{k,\lambda} d_{g,\lambda}^{\mathrm{sub}} + Q_{k,\lambda}\mathbf{E}^{\mathrm{ext}}(t) \tag{3b}$$

Here, the subscript α indexes different nuclei, and $\mathbf{F}_\alpha^{(0)}$ denotes the force on each nucleus outside a cavity. Moreover,

$$\mathbf{F}_\alpha^{\mathrm{cav}} = -\sum_{k,\lambda} \left(\tilde{\epsilon}_{k,\lambda}\tilde{\tilde{q}}_{k,\lambda} + \frac{\tilde{\epsilon}_{k,\lambda}^{\,2}}{m_{k,\lambda}\omega_{k,\lambda}^{\,2}} d_{g,\lambda}^{\mathrm{sub}} \right) \frac{\partial d_{g,\lambda}^{\mathrm{sub}}}{\partial \mathbf{R}_\alpha} \tag{4}$$

denotes the cavity force on each nucleus. In eq 3b, the effective charge of the cavity modes, $Q_{k,\lambda}$, is a phenomenological quantity that describes the coupling coefficient between the cavity mode and the time-dependent external field $\mathbf{E}^{\mathrm{ext}}(t)$. The $Q_{k,\lambda}\mathbf{E}^{\mathrm{ext}}(t)$ term was not defined in the Hamiltonian in eq 1 and is introduced here to phenomenologically describe the external pumping of the cavity modes. From a physical perspective, this term represents an external time-dependent charge current in the normal-mode representation of Maxwell's equations.[43] The $Q_{k,\lambda}\mathbf{E}^{\mathrm{ext}}(t)$ term also corresponds to the input mode in the input−output theory of quantum optics.[44,45] Although the value of $Q_{k,\lambda}$ should be an intrinsic property of an optical cavity, throughout this article, we set $Q_{k,\lambda}$ as 0.1 a.u. for simplicity. Although previous CavMD simulations usually excite polaritons by pumping the molecular subsystem,[29,41] here the polaritons are excited by pumping the cavity mode. These two approaches have been found to yield similar results for the polariton relaxation dynamics,[46] as long as the coherent energy exchange between the molecular bright state and the cavity mode, as quantified by the Rabi splitting, is much faster than either the cavity loss or the molecular dissipation.

In order to propagate the time-dependent CavMD dynamics governed by eq 3, we need to evaluate three key quantities: $\mathbf{F}_\alpha^{(0)}$, $d_{g,\lambda}^{\mathrm{sub}}$, and $\partial d_{g,\lambda}^{\mathrm{sub}}/\partial \mathbf{R}_\alpha$. Previous CavMD studies used empirical MM force fields,[27] for which each atom is assigned a fixed point charge Q_α. At this level of theory, $\mathbf{F}_\alpha^{(0)}$ can be easily evaluated by standard MD packages, and the dipole moment and dipole derivatives can also be calculated in a straightforward manner:

$$d_{g,\lambda}^{\mathrm{sub}} = \sum_\alpha Q_\alpha \mathbf{R}_\alpha \cdot \boldsymbol{\xi}_\lambda \tag{5a}$$

$$\frac{\partial d_{g,\lambda}^{\mathrm{sub}}}{\partial R_{\alpha i}} = Q_\alpha \mathbf{e}_i \cdot \boldsymbol{\xi}_\lambda \tag{5b}$$

where $i = x, y, z$ indexes the Cartesian components of the nuclear coordinates and $\mathbf{R}_\alpha = (R_{\alpha x}, R_{\alpha y}, R_{\alpha z})$. Because the computational cost of evaluating eqs 4 and 5 is marginal compared with calculating $\mathbf{F}_\alpha^{(0)}$, the computational cost of CavMD with MM force fields is similar to the cost of conventional MD outside the cavity.

Independent Bath Approximation. As illustrated in Figure 1, when a dilute solution under VSC is considered, we invoke the independent bath approximation. Under this approximation, the classical cavity modes interact with N_b independent molecular systems, each of which is treated with the standard QM/MM scheme; i.e., a single QM molecule is immersed in a bath of solvent molecules described by an MM force field, and the interaction between the QM and MM systems can be treated with either mechanical embedding[47] or electrostatic embedding.[32] Within this QM/MM treatment, the nuclear forces outside the cavity, $\mathbf{F}_\alpha^{(0)}$, are standard outputs of QM/MM packages. For mechanical embedding treatments, the total dipole moment and dipole derivatives may be expressed as

$$d_{g,\lambda}^{\mathrm{sub}} = \sum_{\beta=1}^{N_b} \left(d_{g,\lambda}^{\beta,\mathrm{QM}} + d_{g,\lambda}^{\beta,\mathrm{MM}} \right) \tag{6a}$$

$$\frac{\partial d_{g,\lambda}^{\mathrm{sub}}}{\partial R_{\alpha i}^{\beta}} = \begin{cases} \dfrac{\partial d_{g,\lambda}^{\beta,\mathrm{QM}}}{\partial R_{\alpha i}^{\beta}} & \text{if } \alpha \in \mathrm{QM} \\ Q_\alpha^{\beta} \mathbf{e}_i \cdot \boldsymbol{\xi}_\lambda & \text{if } \alpha \in \mathrm{MM} \end{cases} \tag{6b}$$

In eq 6a, $\beta = 1, 2, \ldots, N_b$ indexes different independent molecular systems, and in each independent molecular system the total dipole moment is simply the sum of the QM dipole moment $d_{g,\lambda}^{\beta,\mathrm{QM}}$ and the MM dipole moment $d_{g,\lambda}^{\beta,\mathrm{MM}}$, the latter of which is calculated by eq 5a. In eq 6b, for the QM dipole derivatives $\partial d_{g,\lambda}^{\beta,\mathrm{QM}}/\partial R_{\alpha i}^{\beta}$, the off-diagonal components such as $\partial d_{g,x}^{\beta,\mathrm{QM}}/\partial R_{\alpha z}^{\beta}$ (when $\lambda = x$ and $i = z$) are usually nonzero. This behavior is very different from the MM dipole derivatives $Q_\alpha^{\beta}\mathbf{e}_i\cdot\boldsymbol{\xi}_\lambda$, which is always zero when $i \neq \lambda$. Note that eq 6b is exact for mechanical embedding but would need to be modified for electrostatic embedding QM/MM implementations.

Although the solvent molecules are treated with MM force fields, eq 6 guarantees that both the solute and the solvent molecules interact with the cavity modes. If the solvent molecules do not form VSC due to a lack of vibrational modes near the frequencies of the cavity modes, we may further replace the MM contributions in eq 6 with zeros.

With the independent bath approximation, the computational cost scales linearly with the number of QM molecules. Moreover, because the gradients in each local bath can be computed in parallel, first-principles CavMD can be used to simulate collective VSC with an acceptable computational cost. For our simulations, the QM/MM CavMD approach is implemented by interfacing the molecular dynamics package i-PI[48] with the stand-alone QM/MM gradients in Q-Chem.[49,50]

Simulation Details. As an illustrative example of QM/MM CavMD, we simulate the VSC effects on a dilute solution of $Fe(CO)_5$ in n-dodecane solvent at 300 K. For this system, as depicted in Figure 1, VSC is formed between a cavity mode (with both x- and y-polarizations) and the CO vibrations of the $Fe(CO)_5$ molecules. Under the independent bath approximation, we include 16 QM $Fe(CO)_5$ molecules described by density functional theory (DFT) with the BP86[51] functional and def2-mSVP[52] basis set. Each $Fe(CO)_5$ molecule is surrounded by 50 MM n-dodecane molecules described by the OPLS-AA[53] force field. A two-layer ONIOM model with mechanical embedding[47] is used to characterize the interaction

https://doi.org/10.1021/jacs.2c10170
J. Am. Chem. Soc. XXXX, XXX, XXX−XXX

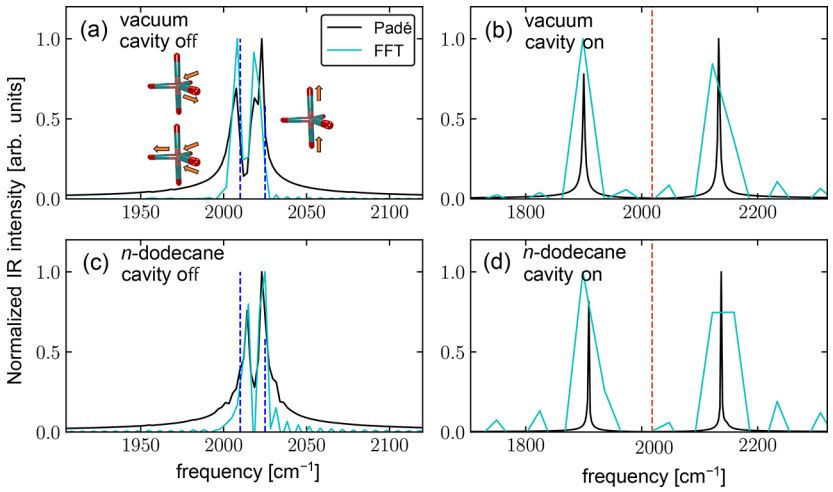

Figure 2. (a) IR spectrum of a single $Fe(CO)_5$ in a vacuum outside the cavity evaluated by Fourier transforming the dipole autocorrelation function. The Padé transform (solid black line) of the autocorrelation function exhibits much better frequency resolution than the fast Fourier transform (solid cyan line). The vertical dashed lines denote the IR spectrum evaluated by a Hessian calculation in vacuum. The inset shows the axial and equatorial modes, which are linear combinations of CO stretch modes. (b) Corresponding polariton spectrum when 16 independent, noninteracting $Fe(CO)_5$ molecules in a vacuum are coupled to the cavity mode at $\omega_c = 2018$ cm^{-1} (vertical dashed red line). (c, d) Same plots as the upper panel except that the solvent environment is explicitly modeled by MM *n*-dodecane molecules.

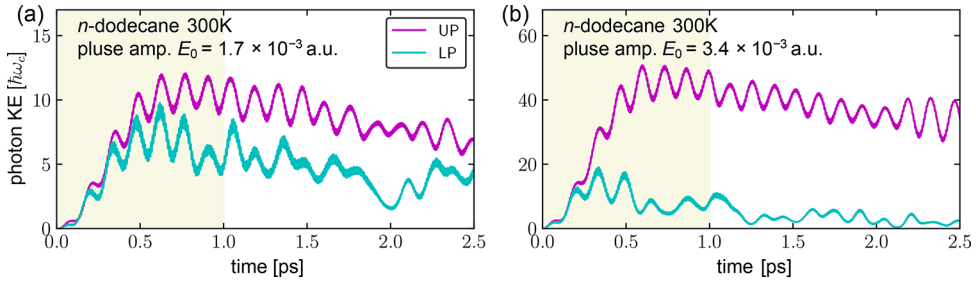

Figure 3. (a) Kinetic energy dynamics of cavity photons under Gaussian pumping of the UP (magenta curve) or LP (cyan curve). The shadowed yellow window represents the time domain during which the Gaussian pulse is turned on. Because the cavity loss rate is assumed to be zero, the decay of the photonic energy indicates polariton relaxation to the dark modes. (b) Same plot as (a) except that the pulse amplitude is doubled. Although the UP dynamics remains similar as in (a), the LP dissipation is greatly accelerated, implicating the LP-enhanced molecular nonlinear absorption mechanism. Each data point here has been smoothed using adjacent averaging over 40 fs windows to remove the fast oscillations in the kinetic energy.

between the QM and MM regions. No cavity loss is included in these simulations. Note that including only 16 $Fe(CO)_5$ molecules in the simulation is expected to yield similar short-time polariton relaxation dynamics as would be obtained for a large number of molecules under VSC, as long as the Rabi splitting is the same for the two cases. This convergent behavior was shown previously with MM force fields,[46] and the current QM/MM results are expected to behave similarly. See the Supporting Information for more simulation details.

RESULTS AND DISCUSSION

Polariton Spectrum. Before presenting the polariton spectrum, we focus on the IR spectrum of $Fe(CO)_5$ in a vacuum. As shown in Figure 2a, for a single $Fe(CO)_5$ in a vacuum at 300 K, the IR spectrum of this molecule is calculated by evaluating the Fourier transform of the dipole autocorrelation function from a 10 ps NVE (constant number of particles, volume, and energy) trajectory. Because the trajectory is relatively short, the direct Fourier transform (solid cyan line) has relatively low resolution. A Padé approximation[54,55] of the Fourier transform (solid black line) provides higher resolution. Both simulated spectra show a two-peak feature near 2000 cm^{-1}, where the lower frequency peak reflects the doubly degenerate equatorial CO vibration with e' symmetry and the higher frequency peak reflects the axial CO vibration with a_2'' symmetry;[39] see the cartoons inserted in Figure 2a for the corresponding vibrational normal modes. The peak positions from the dipole autocorrelation function agree with the Hessian calculation of a single $Fe(CO)_5$ at its equilibrium geometry, as indicated by the dashed vertical blue lines (at 2010 cm^{-1} for the e' vibration and 2025 cm^{-1} for the a_2'' vibration). The heights of the dashed vertical blue lines are proportional to the IR intensities from the Hessian calculation.

Next we investigate 16 randomly oriented $Fe(CO)_5$ molecules in vacuum coupled to the cavity mode with the coupling strength $\tilde{\varepsilon} = 10^{-4}$ a.u., which, according to eq 2, corresponds to a cavity volume of $\Omega = N_{cell} m_c \omega_c^2 / \tilde{\varepsilon}^2 \epsilon_0 \sim 10\, N_{cell}$ nm^3. Figure 2b plots the polariton spectrum by Fourier-transforming the photon autocorrelation function calculated from a 1 ps CavMD simulation. The cavity mode frequency of $\omega_c = 2018$ cm^{-1} is indicated by the vertical dashed red line. Although such a short trajectory cannot provide sufficient frequency resolution when a direct Fourier transform (solid cyan line) is applied, the Padé approximation predicts the formation of a LP and an UP, with frequencies at $\omega_{LP} = 1900$ cm^{-1} and $\omega_{UP} = 2133$ cm^{-1}, respectively. The relative heights of the UP and LP predicted by FFT and the Páde approximation are slightly different, most likely due to the fitting error introduced by the

https://doi.org/10.1021/jacs.2c10170
J. Am. Chem. Soc. XXXX, XXX, XXX−XXX

Páde approximation. The middle polariton (MP) formed by the two vibrational modes coupled to one cavity mode,[6] which is usually very weak, cannot be identified from this short trajectory.

The corresponding spectra obtained when the *n*-dodecane solvent molecules are included in the simulation are plotted in Figures 2c,d. The spectra computed both inside and outside the cavity in the presence of *n*-dodecane are changed only slightly compared to the analogous vacuum spectra. Specifically, inside the cavity, the LP and UP frequencies become $\omega_{LP} = 1909\ cm^{-1}$ and $\omega_{UP} = 2137\ cm^{-1}$, which gives a Rabi splitting of $\Omega_R = 228\ cm^{-1}$, compared to $\Omega_R = 233\ cm^{-1}$ in a vacuum. The relatively small impact of solvent on these IR spectra is understandable, given that *n*-dodecane is a nonpolar solvent.

Polariton Relaxation Dynamics. After obtaining the polariton spectrum, we explore the nonequilibrium polaritonic dynamics for the dilute solution of $Fe(CO)_5$ in *n*-dodecane. The nonequilibrium polaritonic dynamics is initialized by pumping the cavity mode with a Gaussian pulse:

$$\mathbf{E}(t) = \mathbf{e}_x E_0 \sin(\omega t) \exp[-2\ln(2)(t/\tau)^2] \quad (7)$$

This pulse was applied during the time window $0 < t < 1$ ps with a width of $\tau = 0.5$ ps.

First, we simulate the nonequilibrium relaxation dynamics when the amplitude of the Gaussian pulse is set as $E_0 = 1.7 \times 10^{-3}$ a.u. Figure 3a plots the photon kinetic energy ($\sum_{k,\lambda} p_{k,\lambda}^2/2m_{k,\lambda}$) dynamics when either the UP (magenta line) or the LP (cyan line) is pumped. At this pumping amplitude, both the UP and LP excitations demonstrate similar energy gain and relaxation dynamics. The oscillations of the photonic signals have a period of ∼0.15 ps, which reflects the coherent energy transfer between the cavity photon and molecular bright state, in agreement with the Rabi splitting ($\Omega_R = 228\ cm^{-1} = 0.146$ ps). At $t = 2.5$ ps, the photonic signals are dissipated to half the initial energy. Because cavity loss is assumed to be zero and vibrational energy relaxation to the ground state is much slower than a few picoseconds, the photonic energy relaxation on a picosecond time scale after the Gaussian pulse implies polaritonic energy transfer to the dark modes due to a dephasing mechanism. This dephasing behavior agrees with the previous force field CavMD simulations of liquid CO_2 under VSC (see Figure 3 therein),[41] cross-validating both the QM/MM and force field CavMD approaches, although the previous CavMD simulations did not invoke the independent bath approximation.

In these simulations, the molecules are rotating in a manner that changes their orientations and thus influences their coupling to the cavity mode, thereby altering the relative weightings of the molecules in the polaritonic states along the trajectory. In the absence of solvent molecules, the UP dephasing dynamics are found to be greatly suppressed because the solvent phonon modes facilitate relaxation from the UP to the dark modes[34] (see Figure S1 in the Supporting Information). In contrast, the LP dephasing dynamics are similar in the gas phase and solution for this system, suggesting that the dominant relaxation pathways from the LP state are influenced mainly by vibrational anharmonicity of the solute. Pumping the UP state allows relaxation to the dark modes, but subsequent relaxation to the LP state is entropically unfavorable because the number of dark modes is much larger than the single LP state. Pumping the LP state allows relaxation to the dark modes when the Rabi splitting is less than or approximately equal to the thermal energy,[29] as is the case in this study. Polariton relaxation dynamics when the Rabi splitting is much larger than room temperature or in a polar solvent environment will be interesting to explore.

Qualitatively different behavior is observed when the pulse amplitude is increased by a factor of 2. Figure 3b plots the corresponding photon kinetic energy dynamics after pumping the LP or the UP with this stronger pulse. The UP dynamics remains similar to the dynamics observed for the weak pumping case, except that the maximal value is increased by a factor of 4 and the decay is slightly slower. In contrast, the LP decay dynamics becomes much faster than the dynamics in Figure 3a. The fast LP decay under strong pumping has also been observed in force field CavMD simulations of liquid CO_2 under VSC[41] and has been shown to be caused by the LP-enhanced molecular nonlinear absorption mechanism.[41,56−58]

This nonlinear mechanism can be understood in both quantum and classical mechanical pictures. From the quantum mechanical perspective, because molecular vibrations are anharmonic, it is possible to prepare a cavity setup such that twice the LP frequency roughly matches the $0 \rightarrow 2$ vibrational transition. In this case, under strong excitation, the energy of two LP quanta can be directly transferred to the second excited vibrational state of individual molecules. Thus, this nonlinear mechanism provides an additional decay channel for the LP, leading to a shorter LP lifetime under strong excitation. From the classical perspective, LP-enhanced molecular nonlinear absorption can be understood as a "self-catalysis" mechanism: once an individual molecular vibration gains energy during the LP dephasing, its instantaneous vibrational frequency becomes red-shifted due to anharmonicity, causing a larger spectral overlap with the LP and leading to an even faster energy loss of the LP.

Polariton Induced Energy Transfer. After studying the polaritonic energy dynamics following Gaussian pumping, we investigate the CO vibrational energy distribution among the $Fe(CO)_5$ molecules during the polariton relaxation. As a control, Figure 4a plots the kinetic energy statistics of each local CO group in all $Fe(CO)_5$ molecules in the absence of polariton pumping. The equatorial and axial CO groups are indicated by the red and gray bars, respectively. In order to reduce the thermal noise, the kinetic energy of each CO group is calculated by averaging the kinetic energies of the C plus O atoms during a 0.5 ps time window. As expected, under thermal conditions, both the equatorial and axial CO groups exhibit a Maxwell−Boltzmann distribution centered at $\sim 3k_BT = 626\ cm^{-1}$, which is equal to the thermal kinetic energy of each CO group at 300 K. The kinetic energy ratio between all equatorial and all axial CO groups is 1.46, in agreement with the fact that each $Fe(CO)_5$ molecule contains three equatorial CO and two axial CO bonds.

Figure 4b plots the transient kinetic energy statistics of each local CO group after strong UP excitation, under the same simulation conditions as Figure 3b. The transient kinetic energy of each CO group is calculated by averaging the kinetic energy of the CO group during the time window $1.25 < t < 1.75$ ps. Compared with the thermal distribution in Figure 4a, the UP pumping causes the kinetic energy distribution to be blue-shifted and broadened. The broadened distribution is centered around 2000 cm^{-1}. In Figure 4b, the kinetic energy ratio between all equatorial and all axial CO groups is 1.57. This ratio implies that compared with the thermal case, exciting the UP does not cause a significantly different vibrational energy distribution between equatorial and axial bonds. This ratio, however, does not indicate that exciting the UP would not cause vibrational energy transfer between the equatorial and axial

https://doi.org/10.1021/jacs.2c10170
J. Am. Chem. Soc. XXXX, XXX, XXX−XXX

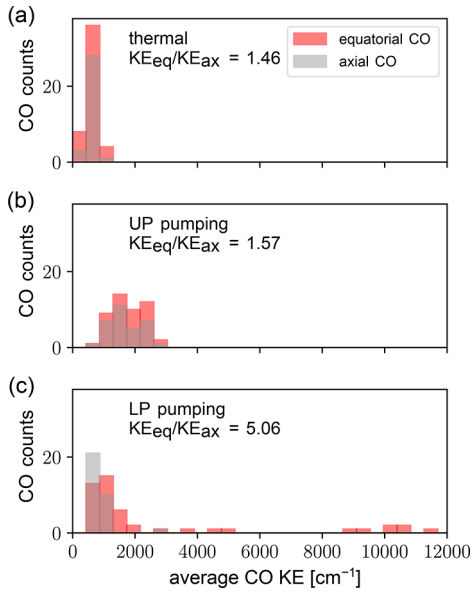

Figure 4. Transient kinetic energy distribution of the CO bonds under three conditions: (a) thermal conditions, (b) UP pumping, and (c) LP pumping. The red bars denote the equatorial CO bonds, and the gray bars denote the axial CO bonds. The simulation conditions under external pumping are the same as for Figure 3b. The transient kinetic energy of each CO group is calculated by averaging over a time window $1.25 < t < 1.75$ ps to minimize the thermal noise. (c) shows that pumping the LP can selectively excite the equatorial bonds.

bonds. The weights of the various vibrations in the polariton state, as quantified by the Hopfield coefficients,[6] can be very different from the population of each vibration after the polariton relaxation. This difference can be used to quantify the magnitude of polariton induced vibrational energy transfer. According to the simple three-state model in the Supporting Information, the ratio of Hopfield coefficients for the equatorial and axial vibrations is 1.33. The larger ratio in Figure 4b might indicate an 18% (i.e., 1.57/1.33 − 1) enhancement in vibrational energy transfer from the axial to the equatorial vibration. In order to obtain a more accurate estimation of the polariton effect on vibrational energy transfer, more extensive simulations are needed to reduce the thermal noise.

Analogous to the study of the UP excitation, Figure 4c plots the corresponding transient vibrational energy statistics of the CO groups after LP excitation, under the same simulation conditions as Figure 3b. In contrast to Figure 4b, we observe a very different vibrational energy distribution between the equatorial (red bars) and axial (gray bars) CO groups. The kinetic energy ratio between all equatorial and all axial CO groups now becomes 5.06, which surpasses both the thermal and UP pumping cases by more than a factor of 2. This value is also much larger than the Hopfield coefficients ratio, which is 2.2 as calculated in the Supporting Information, showing significant vibrational energy transfer from the axial to the equatorial vibration caused by the LP pumping.

Moreover, the equatorial CO groups now dominate the high-energy tail of the distribution, showing that the equatorial CO groups are more likely to be strongly excited. This selective excitation of the equatorial groups, which is reminiscent of a previous finding of selective excitation of the solute molecules after strong solvent LP pumping,[46] is likely to result from the LP-enhanced molecular nonlinear absorption mechanism. Compared with the axial CO group, the slightly lower vibrational frequency of the equatorial CO group appears to cause a stronger interaction with the LP, which in turn leads to more vibrational energy redistribution toward the high-energy tail.

Chemical Dynamics under Polariton Relaxation. Beyond the energy transfer analysis, the real advantage of QM/MM CavMD is the ability to simulate chemical reaction dynamics under VSC. At room temperature, $Fe(CO)_5$ can undergo geometry isomerization by exchanging the two axial CO ligands with two of the equatorial CO ligands, known as the Berry pseudorotation reaction,[39,40] as shown in the inset of Figure 5. Although it does not involve bond breaking and

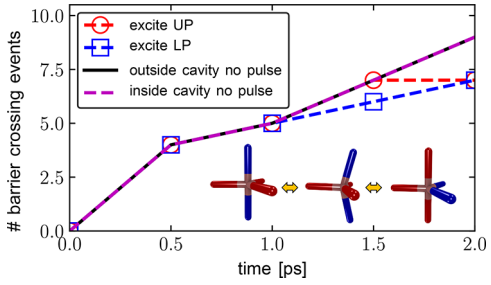

Figure 5. Number of barrier crossing events during $Fe(CO)_5$ pseudorotation as a function of simulation time. Four cases are compared: outside (solid black) and inside (dashed magenta) the cavity under thermal conditions and exciting the UP (dashed red) or the LP (dashed blue) inside the cavity. The initial coordinates and velocities for all molecules in the 16 independent molecular systems are the same for the four cases.

formation, this isomerization process can be regarded as a simple chemical "reaction", which involves a low-energy transition state and occurs on a picoseconds time scale.[40] Such a fast geometry isomerization can be tracked on the fly by 2D-IR spectroscopy[40] and can also be observed during our QM/MM simulations.

Figure 5 plots the number of barrier crossing events during the pseudorotation as a function of time for the simulation outside (solid black) and inside (dashed magenta) the cavity in the absence of external pumping. Without pumping, the reaction dynamics inside and outside the cavity are the same, showing that VSC under thermal conditions does not modify the Berry pseudorotation reaction. Under external pumping of the UP (dashed red) or the LP (dashed blue), the Berry pseudorotation reaction seems to slow down slightly. Because the initial states (i.e., the coordinates and velocities) of the molecules for all the simulations in Figure 5 are exactly the same and the simulations are performed deterministically under an NVE ensemble, such a difference indicates that the IR photochemical dynamics can be tuned by pumping polaritons. This cavity suppression of the pseudorotation is consistent with observations from the recent 2D-IR experiments.[37] Due to the relatively small number of independent molecular systems studied, however, these results are not statistically reliable for comparison to experiments and should be viewed only qualitatively. One possible explanation of the polariton effect on pseudorotation is a solvent effect, in which polariton relaxation to the dark modes excites the low-frequency phonon modes of the nearby solvent molecules, which in turn hinder the pseudorotation dynamics. Another possible explanation is that excitation of other molecular modes of the $Fe(CO)_5$ hinders the pseudorotation dynamics. To investigate these potential mechanisms, more trajectories and additional analyses are required.

https://doi.org/10.1021/jacs.2c10170
J. Am. Chem. Soc. XXXX, XXX, XXX−XXX

Lastly, although LP pumping can create highly excited equatorial vibrations, as compared to the case of UP pumping, generating these highly excited CO vibrations does not appear to significantly modify the pseudorotation dynamics (see Figures 4 and 5). These findings are not contradictory because pseudorotation is controlled by the rotation of the Fe−C bonds, and excitation of the CO vibrations is not expected to significantly modify these Fe−C rotations.

CONCLUSION

This paper presents the QM/MM CavMD scheme for describing chemical dynamics under collective VSC and the application of this approach to a dilute solution of $Fe(CO)_5$ in *n*-dodecane under VSC, which has been studied experimentally.[37] According to the simulations, external pumping of the polariton leads to polariton dephasing to the dark modes as well as polariton-enhanced molecular nonlinear absorption.[41] Moreover, after strong pumping of the LP, the vibrational energy was found to transfer preferably to the equatorial CO vibrations rather than the axial CO vibrations, causing the equatorial vibrational modes to become highly excited. This nontrivial energy transfer pathway highlights the complexity of vibrational energy transfer dynamics under polariton pumping. These QM/MM CavMD simulations also suggest that pumping polaritons could potentially suppress the Berry pseudorotation dynamics.

The recent 2D-IR experiments and accompanying analysis[37] of $Fe(CO)_5$ solution under VSC focused on the dynamics after the initial polariton relaxation (i.e., after ∼2 ps). Our simulations of the short-time polariton relaxation stage (i.e., within ∼2 ps) provide insights into the distribution of vibrational modes following the polariton relaxation over the initial 2 ps. This distribution is expected to influence the subsequent dynamics studied experimentally. Moreover, these simulations may assist future interpretations of the shorter time scale spectroscopic data, which is challenging. Additional simulations and further analysis may provide an explanation for the experimentally observed and computationally suggested suppression of the Berry pseudorotation dynamics. Beyond this specific system, the QM/MM CavMD approach developed in this work provides a numerical tool for exploring the possibility of using VSC to achieve selective IR photochemistry in the liquid phase.

ASSOCIATED CONTENT

Data Availability Statement

The source code, input files, and related tutorials are available at Github (https://github.com/TaoELi/cavity-md-ipi).

Supporting Information

The Supporting Information is available free of charge at https://pubs.acs.org/doi/10.1021/jacs.2c10170.

Additional simulation details; three-state Hopfield model for calculating the Hopfield coefficients for each polariton; polariton relaxation dynamics for $Fe(CO)_5$ in a vacuum; CavMD simulations of VSC effects on single-molecule isomerization reaction (PDF)

AUTHOR INFORMATION

Corresponding Authors

Tao E. Li − *Department of Chemistry, Yale University, New Haven, Connecticut 06520, United States;* orcid.org/0000-0003-0361-5687; Email: tao.li@yale.edu

Sharon Hammes-Schiffer − *Department of Chemistry, Yale University, New Haven, Connecticut 06520, United States;* orcid.org/0000-0002-3782-6995; Email: sharon.hammes-schiffer@yale.edu

Complete contact information is available at: https://pubs.acs.org/10.1021/jacs.2c10170

Notes

The authors declare no competing financial interest.

ACKNOWLEDGMENTS

This material is based upon work supported by the Air Force Office of Scientific Research under AFOSR Award FA9550-18-1-0134. We thank Dr. Tengteng Chen and Prof. Wei Xiong for useful discussions.

REFERENCES

(1) Shalabney, A.; George, J.; Hutchison, J.; Pupillo, G.; Genet, C.; Ebbesen, T. W. Coherent Coupling of Molecular Resonators with a Microcavity Mode. *Nat. Commun.* **2015**, *6*, 5981.

(2) Long, J. P.; Simpkins, B. S. Coherent Coupling between a Molecular Vibration and Fabry-Perot Optical Cavity to Give Hybridized States in the Strong Coupling Limit. *ACS Photonics* **2015**, *2*, 130−136.

(3) Thomas, A.; George, J.; Shalabney, A.; Dryzhakov, M.; Varma, S. J.; Moran, J.; Chervy, T.; Zhong, X.; Devaux, E.; Genet, C.; Hutchison, J. A.; Ebbesen, T. W. Ground-State Chemical Reactivity under Vibrational Coupling to the Vacuum Electromagnetic Field. *Angew. Chemie Int. Ed.* **2016**, *55*, 11462−11466.

(4) Thomas, A.; Lethuillier-Karl, L.; Nagarajan, K.; Vergauwe, R. M. A.; George, J.; Chervy, T.; Shalabney, A.; Devaux, E.; Genet, C.; Moran, J.; Ebbesen, T. W. Tilting a Ground-State Reactivity Landscape by Vibrational Strong Coupling. *Science* **2019**, *363*, 615−619.

(5) Joseph, K.; Kushida, S.; Smarsly, E.; Ihiawakrim, D.; Thomas, A.; Paravicini-Bagliani, G. L.; Nagarajan, K.; Vergauwe, R.; Devaux, E.; Ersen, O.; Bunz, U. H. F.; Ebbesen, T. W. Supramolecular Assembly of Conjugated Polymers under Vibrational Strong Coupling. *Angew. Chemie Int. Ed.* **2021**, *60*, 19665−19670.

(6) Xiang, B.; Ribeiro, R. F.; Du, M.; Chen, L.; Yang, Z.; Wang, J.; Yuen-Zhou, J.; Xiong, W. Intermolecular Vibrational Energy Transfer Enabled by Microcavity Strong Light−Matter Coupling. *Science* **2020**, *368*, 665−667.

(7) Imperatore, M. V.; Asbury, J. B.; Giebink, N. C. Reproducibility of Cavity-Enhanced Chemical Reaction Rates in the Vibrational Strong Coupling Regime. *J. Chem. Phys.* **2021**, *154*, 191103.

(8) Wiesehan, G. D.; Xiong, W. Negligible Rate Enhancement from Reported Cooperative Vibrational Strong Coupling Catalysis. *J. Chem. Phys.* **2021**, *155*, 241103.

(9) Li, T. E.; Cui, B.; Subotnik, J. E.; Nitzan, A. Molecular Polaritonics: Chemical Dynamics Under Strong Light-Matter Coupling. *Annu. Rev. Phys. Chem.* **2022**, *73*, 43−71.

(10) Fregoni, J.; Garcia-Vidal, F. J.; Feist, J. Theoretical Challenges in Polaritonic Chemistry. *ACS Photonics* **2022**, *9*, 1096−1107.

(11) Wang, D. S.; Yelin, S. F. A Roadmap Toward the Theory of Vibrational Polariton Chemistry. *ACS Photonics* **2021**, *8*, 2818−2826.

(12) Sidler, D.; Schäfer, C.; Ruggenthaler, M.; Rubio, A. Polaritonic Chemistry: Collective Strong Coupling Implies Strong Local Modification of Chemical Properties. *J. Phys. Chem. Lett.* **2021**, *12*, 508−516.

(13) Galego, J.; Climent, C.; Garcia-Vidal, F. J.; Feist, J. Cavity Casimir-Polder Forces and Their Effects in Ground-State Chemical Reactivity. *Phys. Rev. X* **2019**, *9*, 021057.

(14) Campos-Gonzalez-Angulo, J. A.; Ribeiro, R. F.; Yuen-Zhou, J. Resonant Catalysis of Thermally Activated Chemical Reactions with Vibrational Polaritons. *Nat. Commun.* **2019**, *10*, 4685.

(15) Li, X.; Mandal, A.; Huo, P. Cavity Frequency-Dependent Theory for Vibrational Polariton Chemistry. *Nat. Commun.* **2021**, *12*, 1315.

(16) Fischer, E. W.; Saalfrank, P. Ground State Properties and Infrared Spectra of Anharmonic Vibrational Polaritons of Small Molecules in Cavities. *J. Chem. Phys.* **2021**, *154*, 104311.
(17) Yang, P. Y.; Cao, J. Quantum Effects in Chemical Reactions under Polaritonic Vibrational Strong Coupling. *J. Phys. Chem. Lett.* **2021**, *12*, 9531−9538.
(18) Wang, D. S.; Neuman, T.; Yelin, S. F.; Flick, J. Cavity-Modified Unimolecular Dissociation Reactions via Intramolecular Vibrational Energy Redistribution. *J. Phys. Chem. Lett.* **2022**, *13*, 3317−3324.
(19) Flick, J.; Ruggenthaler, M.; Appel, H.; Rubio, A. Atoms and Molecules in Cavities, from Weak to Strong Coupling in Quantum-Electrodynamics (QED) Chemistry. *Proc. Natl. Acad. Sci. U. S. A.* **2017**, *114*, 3026−3034.
(20) Riso, R. R.; Haugland, T. S.; Ronca, E.; Koch, H. Molecular Orbital Theory in Cavity QED Environments. *Nat. Commun.* **2022**, *13*, 1368.
(21) Schäfer, C.; Flick, J.; Ronca, E.; Narang, P.; Rubio, A. Shining Light on the Microscopic Resonant Mechanism Responsible for Cavity-Mediated Chemical Reactivity. *arXiv*, April 26, **2021**. DOI: DOI: 10.48550/arXiv.2104.12429 (accessed 2021-04-26).
(22) Bonini, J.; Flick, J. Ab Initio Linear-Response Approach to Vibro-polaritons in the Cavity Born-Oppenheimer Approximation. *J. Chem. Theory Comput.* **2022**, *18*, 2764−2773.
(23) Yang, J.; Ou, Q.; Pei, Z.; Wang, H.; Weng, B.; Shuai, Z.; Mullen, K.; Shao, Y. Quantum-Electrodynamical Time-Dependent Density Functional Theory within Gaussian Atomic Basis. *J. Chem. Phys.* **2021**, *155*, 064107.
(24) Philbin, J. P.; Haugland, T. S.; Ghosh, T. K.; Ronca, E.; Chen, M.; Narang, P.; Koch, H. Molecular van der Waals Fluids in Cavity Quantum Electrodynamics. *arXiv*, September 16, **2022**. DOI: DOI: 10.48550/arXiv.2209.07956 (accessed 2022-09-16).
(25) Rosenzweig, B.; Hoffmann, N. M.; Lacombe, L.; Maitra, N. T. Analysis of the Classical Trajectory Treatment of Photon Dynamics for Polaritonic Phenomena. *J. Chem. Phys.* **2022**, *156*, 054101.
(26) Triana, J. F.; Hernández, F. J.; Herrera, F. The Shape of the Electric Dipole Function Determines the Sub-picosecond Dynamics of Anharmonic Vibrational Polaritons. *J. Chem. Phys.* **2020**, *152*, 234111.
(27) Li, T. E.; Subotnik, J. E.; Nitzan, A. Cavity Molecular Dynamics Simulations of Liquid Water under Vibrational Ultrastrong Coupling. *Proc. Natl. Acad. Sci. U. S. A.* **2020**, *117*, 18324−18331.
(28) Li, T. E.; Nitzan, A.; Hammes-Schiffer, S.; Subotnik, J. E. Quantum Simulations of Vibrational Strong Coupling via Path Integrals. *J. Phys. Chem. Lett.* **2022**, *13*, 3890−3895.
(29) Li, T. E.; Nitzan, A.; Subotnik, J. E. Polariton Relaxation under Vibrational Strong Coupling: Comparing Cavity Molecular Dynamics Simulations against Fermi's Golden Rule Rate. *J. Chem. Phys.* **2022**, *156*, 134106.
(30) Luk, H. L.; Feist, J.; Toppari, J. J.; Groenhof, G. Multiscale Molecular Dynamics Simulations of Polaritonic Chemistry. *J. Chem. Theory Comput.* **2017**, *13*, 4324−4335.
(31) Pulay, P. Analytical Derivatives, Forces, Force Constants, Molecular Geometries, and Related Response Properties in Electronic Structure Theory. *WIREs Comput. Mol. Sci.* **2014**, *4*, 169−181.
(32) Senn, H. M.; Thiel, W. QM/MM Methods for Biomolecular Systems. *Angew. Chemie Int. Ed.* **2009**, *48*, 1198−1229.
(33) Shao, Y.; Kong, J. YinYang Atom: A Simple Combined ab Initio Quantum Mechanical Molecular Mechanical Model. *J. Phys. Chem. A* **2007**, *111*, 3661−3671.
(34) del Pino, J.; Feist, J.; Garcia-Vidal, F. J. Quantum Theory of Collective Strong Coupling of Molecular Vibrations with a Microcavity Mode. *New J. Phys.* **2015**, *17*, 053040.
(35) Groenhof, G.; Climent, C.; Feist, J.; Morozov, D.; Toppari, J. J. Tracking Polariton Relaxation with Multiscale Molecular Dynamics Simulations. *J. Phys. Chem. Lett.* **2019**, *10*, 5476−5483.
(36) Tichauer, R. H.; Feist, J.; Groenhof, G. Multi-scale Dynamics Simulations of Molecular Polaritons: The Effect of Multiple Cavity Modes on Polariton Relaxation. *J. Chem. Phys.* **2021**, *154*, 104112.
(37) Chen, T.-T.; Du, M.; Yang, Z.; Yuen-Zhou, J.; Xiong, W. Cavity-enabled Enhancement of Ultrafast Intramolecular Vibrational Redistribution over Pseudorotation. *Science* **2022**, *378*, 790−794.
(38) Nagarajan, K.; Thomas, A.; Ebbesen, T. W. Chemistry under Vibrational Strong Coupling. *J. Am. Chem. Soc.* **2021**, *143*, 16877−16889.
(39) Portius, P.; Bühl, M.; George, M. W.; Grevels, F. W.; Turner, J. J. Structure and Dynamics of Iron Pentacarbonyl. *Organometallics* **2019**, *38*, 4288−4297.
(40) Cahoon, J. F.; Sawyer, K. R.; Schlegel, J. P.; Harris, C. B. Determining Transition-State Geometries in Liquids Using 2D-IR. *Science* **2008**, *319*, 1820−1823.
(41) Li, T. E.; Nitzan, A.; Subotnik, J. E. Cavity Molecular Dynamics Simulations of Vibrational Polariton-enhanced Molecular Nonlinear Absorption. *J. Chem. Phys.* **2021**, *154*, 094124.
(42) Flick, J.; Appel, H.; Ruggenthaler, M.; Rubio, A. Cavity Born−Oppenheimer Approximation for Correlated Electron−Nuclear-Photon Systems. *J. Chem. Theory Comput.* **2017**, *13*, 1616−1625.
(43) Cohen-Tannoudji, C.; Dupont-Roc, J.; Grynberg, G. *Photons and Atoms: Introduction to Quantum Electrodynamics*; Wiley: New York, 1997; pp 280−295.
(44) Gardiner, C. W.; Zoller, P. *A Handbook of Markovian and Non-Markovian Quantum Stochastic Methods with Applications to Quantum Optics*; Springer: Berlin, 2004.
(45) Ribeiro, R. F.; Dunkelberger, A. D.; Xiang, B.; Xiong, W.; Simpkins, B. S.; Owrutsky, J. C.; Yuen-Zhou, J. Theory for Nonlinear Spectroscopy of Vibrational Polaritons. *J. Phys. Chem. Lett.* **2018**, *9*, 3766−3771.
(46) Li, T. E.; Nitzan, A.; Subotnik, J. E. Energy-Efficient Pathway for Selectively Exciting Solute Molecules to High Vibrational States via Solvent Vibration-Polariton Pumping. *Nat. Commun.* **2022**, *13*, 4203.
(47) Vreven, T.; Morokuma, K. *Annual Reports in Computational Chemistry*; Elsevier: 2006; Vol. 2, pp 35−51.
(48) Kapil, V.; et al. I-PI 2.0: A Universal Force Engine for Advanced Molecular Simulations. *Comput. Phys. Commun.* **2019**, *236*, 214−223.
(49) Woodcock, H. L.; Hodošček, M.; Gilbert, A. T. B.; Gill, P. M. W.; Schaefer, H. F.; Brooks, B. R. Interfacing Q-Chem and CHARMM to Perform QM/MM Reaction Path Calculations. *J. Comput. Chem.* **2007**, *28*, 1485−1502.
(50) Epifanovsky, E.; et al. Software for the Frontiers of Quantum Chemistry: An Overview of Developments in the Q-Chem 5 Package. *J. Chem. Phys.* **2021**, *155*, 084801.
(51) Becke, A. D. Density-Functional Exchange-Energy Approximation with Correct Asymptotic Behavior. *Phys. Rev. A* **1988**, *38*, 3098.
(52) Grimme, S.; Brandenburg, J. G.; Bannwarth, C.; Hansen, A. Consistent Structures and Interactions by Density Functional Theory with Small Atomic Orbital Basis Sets. *J. Chem. Phys.* **2015**, *143*, 054107.
(53) Jorgensen, W. L.; Maxwell, D. S.; Tirado-Rives, J. Development and Testing of the OPLS All-Atom Force Field on Conformational Energetics and Properties of Organic Liquids. *J. Am. Chem. Soc.* **1996**, *118*, 11225−11236.
(54) Bruner, A.; Lamaster, D.; Lopata, K. Accelerated Broadband Spectra Using Transition Dipole Decomposition and Padé Approximants. *J. Chem. Theory Comput.* **2016**, *12*, 3741−3750.
(55) Goings, J. J.; Lestrange, P. J.; Li, X. Real-Time Time-Dependent Electronic Structure Theory. *Wiley Interdiscip. Rev.: Comput. Mol. Sci.* **2018**, *8*, e1341.
(56) Xiang, B.; Ribeiro, R. F.; Chen, L.; Wang, J.; Du, M.; Yuen-Zhou, J.; Xiong, W. State-Selective Polariton to Dark State Relaxation Dynamics. *J. Phys. Chem. A* **2019**, *123*, 5918−5927.
(57) Xiang, B.; Xiong, W. Molecular Vibrational Polariton: Its Dynamics and Potentials in Novel Chemistry and Quantum Technology. *J. Chem. Phys.* **2021**, *155*, 050901.
(58) Ribeiro, R. F.; Campos-Gonzalez-Angulo, J. A.; Giebink, N. C.; Xiong, W.; Yuen-Zhou, J. Enhanced Optical Nonlinearities under Collective Strong Light-Matter Coupling. *Phys. Rev. A* **2021**, *103*, 063111.

https://doi.org/10.1021/jacs.2c10170
J. Am. Chem. Soc. XXXX, XXX, XXX−XXX